SUPPLEMENTARY MATERIALS

Aging and reactivity assessment of nanoscale zerovalent iron in groundwater systems

Junmin Deng[a], Tao Chen[a], Yara Arbid[a], Mathieu Pasturel[a], Sungjun Bae[b], Khalil Hanna[a*]

[a] *Univ. Rennes, Ecole Nationale Supérieure de Chimie de Rennes, CNRS, ISCR-UMR 6226, F-35000 Rennes, France*

[b] *Department of Civil and Environmental Engineering, Konkuk University, 120 Neungdong-ro, Gwangjin-gu, Seoul 05029, Republic of Korea*

*Corresponding author: khalil.hanna@ensc-rennes.fr

The following are included as supporting information for this paper:

No. of pages: 19

No. of figures: 8

No. of tables: 5

No. of Text: 3

Text S1.

Chemicals. Sodium borohydride ($NaBH_4$, ≥99.0%), ferric chloride hexahydrate ($FeCl_3 \cdot 6H_2O$, ≥99.0%), hydrochloric acid (HCl, 37%), sodium hydroxide (NaOH, ≥99.0%), *p*-nitrophenol (*p*-NP, ≥99%), *p*-aminophenol (*p*-AP, ≥98%), nalidixic acid (NA, 99.0%), sodium chloride (NaCl, ≥99.5%), sodium sulfate (Na_2SO_4, ≥99.0%), sodium nitrate ($NaNO_3$, ≥99.0%), sodium carbonate (Na_2CO_3, ≥99.5%), sodium metasilicate pentahydrate ($Na_2SiO_3 \cdot 5H_2O$, ≥98.0%), calcium carbonate ($CaCO_3$, ≥99.0%), monobasic potassium phosphate (KH_2PO_4, ≥99.0%), sulfuric acid (H_2SO_4, 95-97%), acetone (CH_3COCH_3, ≥99.5%), oxalic acid ($C_2H_2O_4$, 98%), L-Ascorbic acid ($C_6H_8O_6$, 99%), ammonium molybdate tetrahydrate ($(NH_4)_6Mo_7O_{24} \cdot 4H_2O$, 99.98%), potassium antimony(III) oxide tartrate trihydrate ($K_2(SbO)_2C_8H_4O_{10} \cdot 3H_2O$, ≥99.0%), ethanol ($CH_3CH_2OH$, 96%), phenolphthalein ($C_{20}H_{14}O_4$, ≥99.0%), methyl orange ($C_{14}H_{14}N_3NaO_3S$, ACS reagent, dye content 85%) ethylenediaminetetraacetic acid (EDTA, ≥99%), Eriochrome black T glycerol ($C_{20}H_{12}N_3NaO_7S$, indicator grade), ammonium hydroxide solution (NH_4OH, 28% NH_3 in H_2O), ferrous chloride tetrahydrate ($FeCl_2 \cdot 4H_2O$, ≥99.0%) and 1,10-phenanthroline ($C_{12}H_8N_2 \cdot H_2O$, ≥99.0%) were all purchased from Sigma-Aldrich. Acetonitrile (CH_3CN, 99.99%, Sigma) and acetic acid (CH_3CO_2H, 99.7%, ACROS) were used for mobile phase of high-performance liquid chromatography (HPLC). NA stock solution (5 mM) and ferrous chloride stock solution (100 mM) were prepared with 0.1 M NaOH and 0.1 M HCl, respectively.

Text S2.

Characterization of NZVI particle. NZVI generally formed spherically shaped particles with a diameter of approximately 50−100 nm, which aggregated into a chain-like structure owing to magnetic interactions (Kanel et al. 2007). The SAED pattern of these chain-like aggregates displayed the weak (110, 2,049 Å) and (200, 1,460 Å) reflections, indicating that Fe^0 was poorly crystalline and mostly amorphous (Jorge et al. 2008).

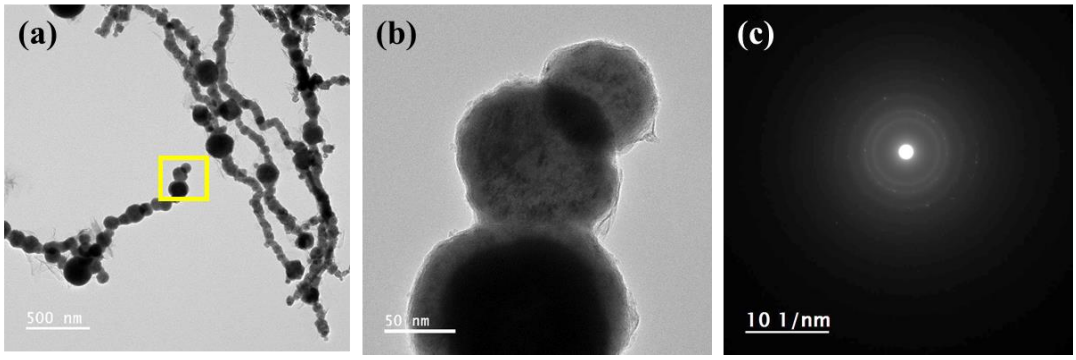

Figure. S1. (a) and (b) TEM images of fresh NZVI; and (c) selective area electron diffraction patterns of a particle.

Table S1. Water quality parameters of the five groundwaters sampled in France used in this study

Water quality parameters	GW1	GW2	GW3	GW4	GW5
pH	8.1	7.7	7.5	7.5	7.5
EC (µS cm^{-1})	488	395	461	515	521
TDS (mg L^{-1})	412	344	500	532	590
TH (equivalent concentration of $CaCO_3$, mg L^{-1})	136	141	299	293	312
TOC (mg L^{-1})	3.1	3.0	1.5	1.7	1.8
TP (mg L^{-1})	<0.1	<0.1	<0.1	<0.1	<0.1
HCO_3^-(mM)	1.50	2.00	4.30	4.30	4.20
Cl^- (mM)	1.50	0.90	0.41	0.99	0.54
SO_4^{2-} (mM)	0.69	0.29	0.19	0.23	0.23
NO_3^- (mM)	0.49	0.18	0.60	0.91	1.26
SiO_3^{2-} (mM)	0.21	0.24	0.09	0.13	0.11
Na^+ (mM)	1.48	1.62	0.29	0.61	0.49
Ca^{2+} (mM)	0.75	0.90	2.61	2.44	2.59
Mg^{2+} (mM)	0.56	0.43	0.37	0.33	0.55
K^+ (mM)	0.30	0.10	0.03	1.01	0.44
Sr (µg L^{-1})	111	107	145	80	235
Zn (µg L^{-1})	58	181	3.5	53	16
B (µg L^{-1})	42	48	16	58	58
Ba (µg L^{-1})	32	7.5	12	16	29
Cu (µg L^{-1})	24	11	1.1	4.5	8.3
Al (µg L^{-1})	3.6	4.7	2.0	1.5	1.0
Li (µg L^{-1})	2.7	3.5	1.3	2.7	2.1
Mn (µg L^{-1})	2.7	11.7	0.1	0.4	0.2
Ni (µg L^{-1})	2.5	7.7	0.3	1.2	2.3
Fe (µg L^{-1})	1.9	4.4	1.7	5.8	0.2
Rb (µg L^{-1})	1.7	0.9	0.6	3.4	2.2
Sc (µg L^{-1})	0.2	0.3	0.2	0.2	0.2
V (µg L^{-1})	0.2	0.5	0.3	0.4	0.5
As (µg L^{-1})	0.2	0.7	0.3	0.4	0.4
Cd (µg L^{-1})	0.1	12	0	0.1	0
Sb (µg L^{-1})	0.1	0.1	0.1	0.1	0.1
Co(µg L^{-1})	0.1	0.2	0.1	0.1	0.1
Cr (µg L^{-1})	0	0.8	0.1	0.4	0.1

Table S2. Summary of the surface complexation model and parameters for the NZVI aging products.

Parameters	Magnetite (Cheng et al. 2018)	Maghemite (Cheng et al. 2018)	Lepidocrocite (Zhang et al. 1992)
Site density (nm^{-2})	1.50	0.99	1.67
Capacitance ($F\ m^{-2}$)	2.10	2.40	2.08
$\equiv FeOH_2^+ \leftrightarrows \equiv FeOH + H^+; pK_{a1}$	5.19	5.39	6.45
$\equiv FeOH \leftrightarrows \equiv FeO^- + H^+; pK_{a2}$	-7.82	-7.51	-8.13

Samples	Specific surface area (SSA, $m^2\ g^{-1}$)	$\log^{NA} K$
PW-anoxic aged NZVI	20	28.0 (magnetite)
GW1-anoxic aged NZVI	24	22.1 (magnetite)
PW-oxic aged NZVI	25	29.2 (magnetite)
GW1-oxic aged NZVI	42	21.4 (maghemite) and 18.8 (lepidocrocite)

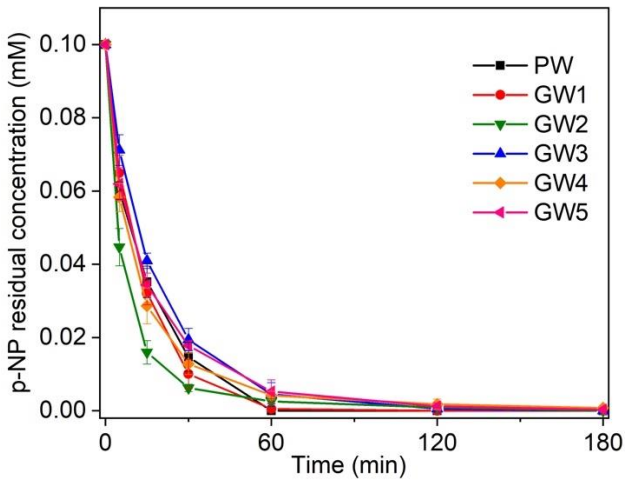

Figure. S2. Removal kinetics of *p*-NP by NZVI in pure water and five groundwaters. Experimental conditions: $[p\text{-NP}]_{initial}$ = 0.1 mM, [NZVI]= 50 mg L^{-1}, reaction pH=9.0±0.2.

Table S3. Final *p*-AP concentration after reaction in different reaction systems. As [*p*-NP]$_{initial}$ = 0.1 mM, concentration close to 0.1 mM means that mass balance is achieved.

Systems	**PW**	**GW1**	**GW2**	**GW3**	**GW4**	**GW5**
***p*-AP concentrations (mM)**	0.098	0.098	0.10	0.099	0.099	0.11

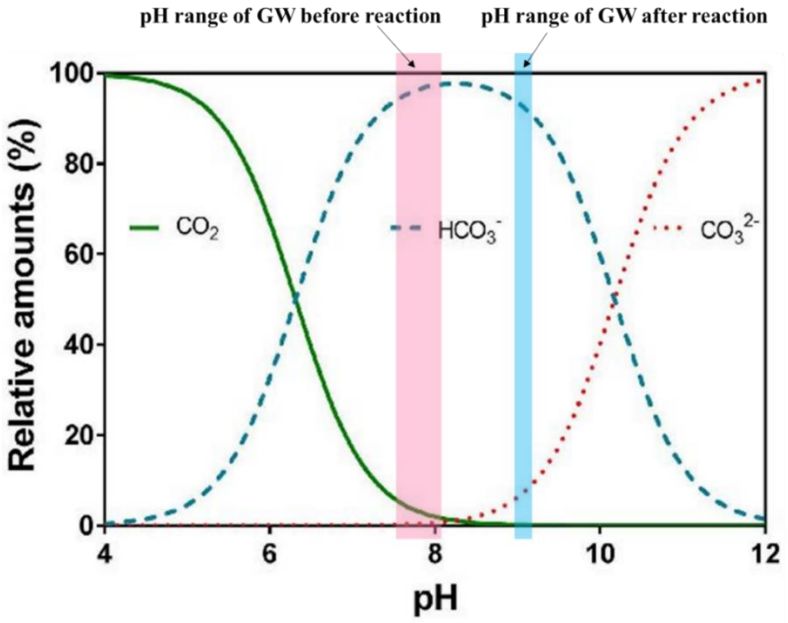

Figure. S3. Concentration of inorganic carbon species changes as a function of pH. The pH ranges of groundwater before and after reaction in this study are shown as pink and blue areas, respectively. Reproduced with permission from (Pedersen et al. 2013), Copyright 2013, Frontiers.

Table S4. Comparison of pH, TOC and anions concentrations in groundwater before and after reaction. Experimental conditions: $[p\text{-NP}]_{initial}$ = 0.1 mM, [NZVI]= 50 mg L^{-1}, reaction pH=9.0±0.2

Anions	Before/after reaction	GW1	GW2	GW3	GW4	GW5
pH	before	8.1	7.7	7.5	7.5	7.5
	after	9.1	9.1	9.1	9.0	9.1
Cl^- (mM)	before	1.50	0.90	0.41	0.99	0.54
	after	1.34	0.81	0.35	0.84	0.48
SO_4^{2-} (mM)	before	0.69	0.29	0.19	0.23	0.23
	after	0.61	0.31	0. 15	0.21	0.22
NO_3^- (mM)	before	0.49	0.18	0.6	0.91	1.26
	after	0.31	0.021	0.38	0.69	1.05
HCO_3^- (mM)	before	1.50	2.01	4.30	4.30	4.20
	after	1.32	1.71	2.71	2.8	3.05
CO_3^{2-} (mM)`	before	0	0	0	0	0
	after	0.12	0.2	0.11	0.12	0
SiO_3^{2-} (mM)	before	0.21	0.24	0.09	0.13	0.11
	after	0.02	0.02	0.003	0.02	0.02
TOC(±0.2) ($mg\ L^{-1}$)	before	3.1	3.0	1.5	1.7	1.8
	after	2.8	2.9	1.5	1.6	1.6

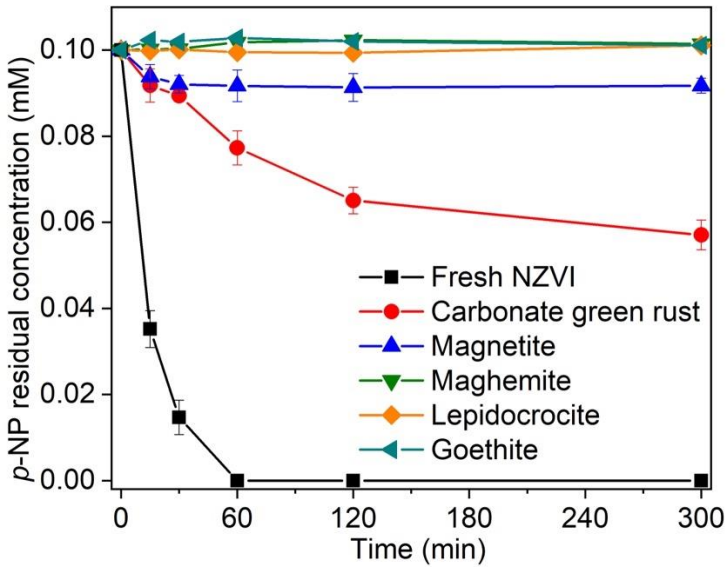

Figure. S4. Removal kinetics of *p*-NP by different iron minerals. Experimental conditions: $[p\text{-NP}]_{initial}$ = 0.1 mM, [minerals]= 50 mg L^{-1}, reaction pH=9.0±0.2.

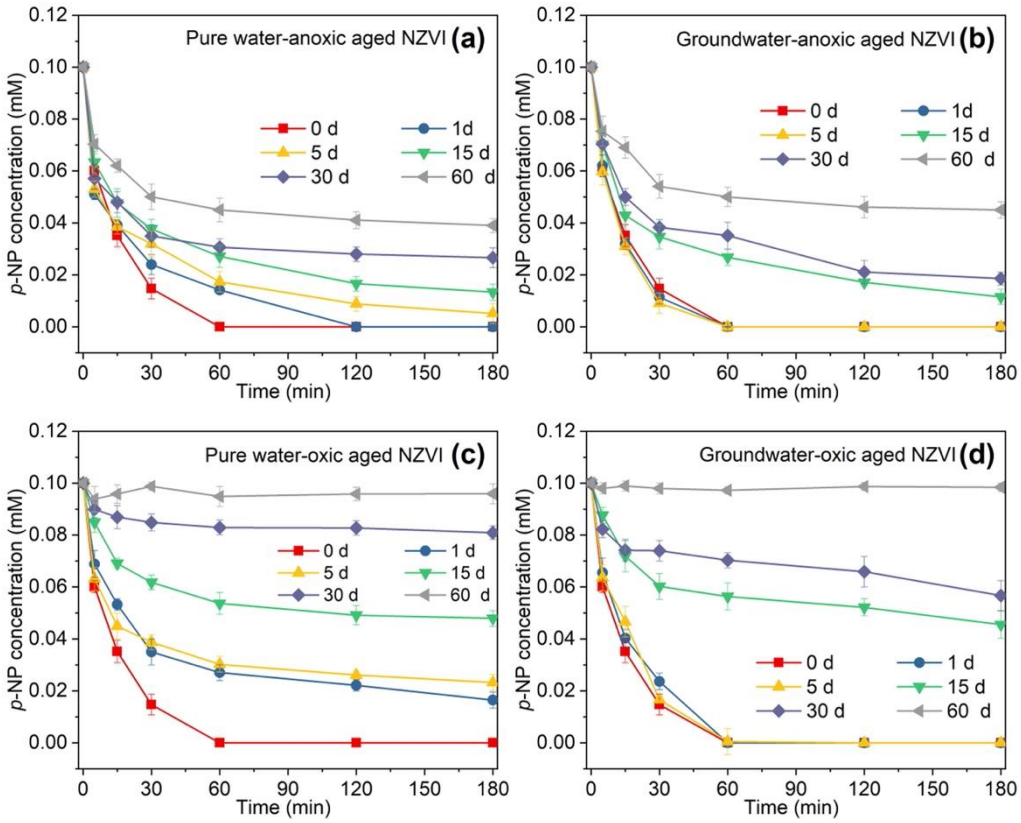

Figure S5. Removal kinetics of *p*-NP by fresh and different aged NZVIs (a) pure water anoxic aged NZVI; (b) groundwater anoxic aged NZVI; (c) pure water oxic aged NZVI; (d) groundwater oxic aged NZVI, Experimental conditions: $[p\text{-NP}]_{initial}$ = 0.1 mM, [NZVI]= 50 mg L^{-1}, reaction pH=9.0±0.2.

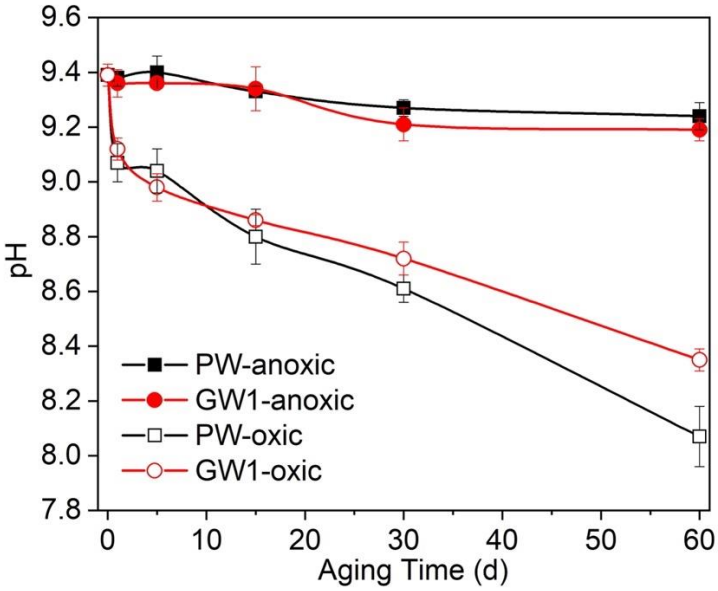

Figure. S6. pH variation of NZVI suspension with aging time at different aging conditions.

Text S3.

Changes in solution chemistry and pH value during NZVI aging process. pH variations along the NZVI aging process were monitored (Figure. S6). A decrease in solution pH during the transformation of NZVI to Fe(II) and/or Fe(III) minerals could be attributed to the oxidation of ferrous ions and hydrolysis of dissolved iron ions (Eqs. 1-3) (Hua et al. 2018, Noubactep 2013).

$$2Fe^{2+} + O_2 + 6H_2O \rightarrow 2Fe_3O_4 + 12H^+ \quad \text{(S1)}$$

$$Fe^{2+} + 3OH^- \rightarrow Fe(OH)_2 \quad \text{(S2)}$$

$$Fe^{3+} + 3OH^- \rightarrow Fe(OH)_3 \quad \text{(S3)}$$

Due to the pH buffer capacity of groundwater (Shao et al. 2015), the pH decrease in groundwater systems was less obvious than that in the pure water system. Interestingly, the suspension pH after oxic aging decreased significantly from 9.4 to 8.1 in pure water and 8.4 in groundwater, while only a little pH fluctuation was observed after anoxic aging. We assume such a big difference in suspension pH under anoxic and oxic conditions was related to O_2-involved reactions. As per Eq. S3, O_2-rich conditions are favorable for the oxidation equation and H^+ generation.

On the other hand, the formation of green rust depends on solution pH.(Abdelmoula et al. 1996, Schwertmann and Fechter 1994) It is reported that carbonate green rust is mostly observed in alkaline conditions (pH 8-13), and neutral to weak base conditions are favorable for its formation (Halevy et al. 2017). With the

ongoing aging process, the suspension became less basic, facilitating the formation of carbonate green rust. However, as high pHs promote the transformation from green rust to magnetite (Guilbaud et al. 2013), magnetite was still the major phase in NZVI aging products.

Interestingly, despite the absence of a carbon source in the original pure water system, a slight amount of carbonate green rust was detected. The formation of carbonate green rust in the pure water system under oxic conditions could be attributed to the dissolution of CO_2 from the atmosphere. According to our experimental data, 0.22 mM HCO_3^- was generated in pure water after 5 h exposure to air with strong stirring. Therefore, the formation of carbonate green rust in the pure water system was mainly controlled by the CO_2 dissolution process. In general, in the PW-oxic system, the increase in carbonate green rust peaks may be induced by the dissolution of CO_2 in water and the decreasing pH along aging time, which is favorable for the formation of carbonate green rust (Halevy et al. 2017).

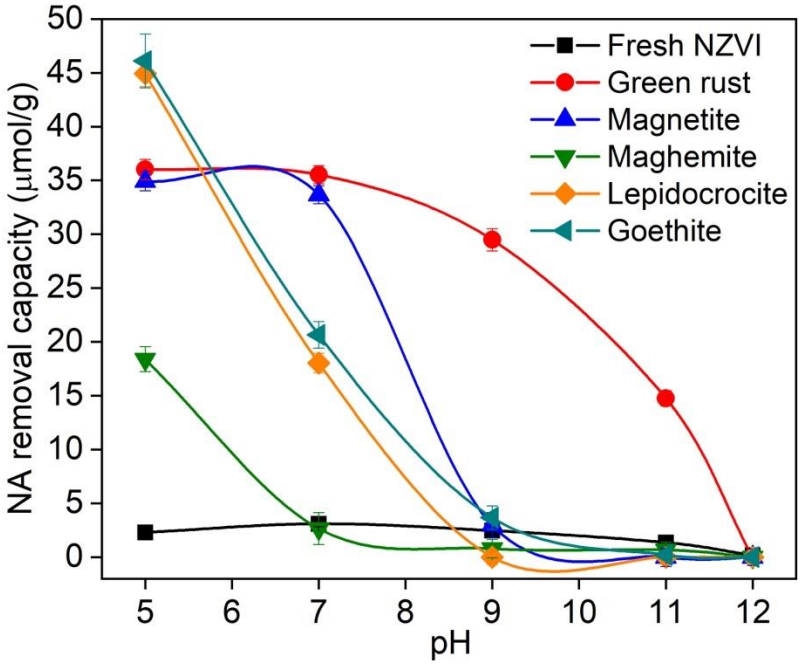

Figure S7. NA adsorption versus pH by fresh NZVI and different iron minerals. Experimental conditions: $[NA]_{initial}$ =10 μM, [minerals]= 50 mg L^{-1}, adsorption duration = 2 hours.

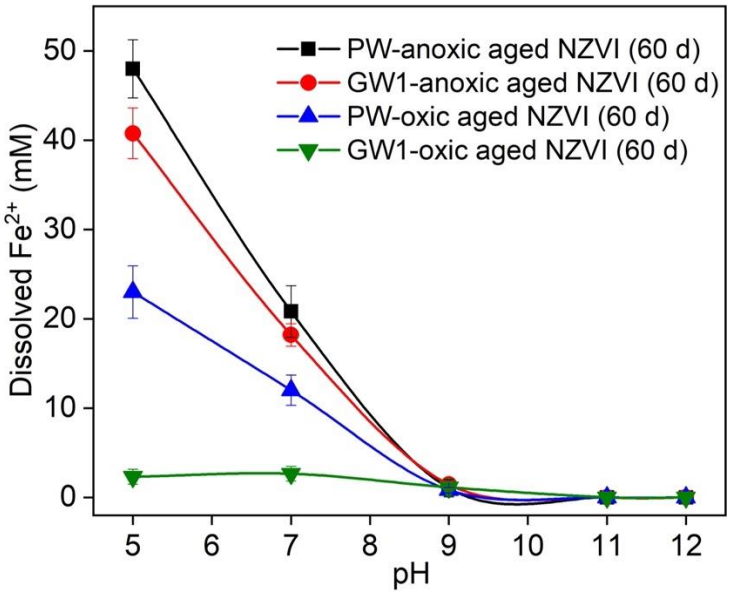

Figure S8. Dissolved Fe (II) concentration during NA adsorption by different aged NZVI at 60 days. Experimental conditions: $[NA]_{initial}$ = 10 µM, [NZVI]= 50 mg L^{-1}, adsorption duration = 2 hours.

Table S5. The compositions of 60 d NZVI aging products under different aging conditions as determined using XRD data.

Aging conditions	**Magnetite/ Maghemite**	**Goethite**	**Carbonate green rust**	**Lepidocrocite**
PW-anoxic	100%	-	-	-
GW1-anoxic	55%	10%	35%	-
PW- oxic	86%	-	14%	-
GW1-oxic	55%	8%	7%	30%

References

Abdelmoula, M., Refait, P., Drissi, S.H., Mihe, J.P. and Génin, J.M.R., 1996. Conversion electron Mössbauer spectroscopy and X-ray diffraction studies of the formation of carbonate-containing green rust one by corrosion of metallic iron in $NaHCO_3$ and ($NaHCO_3$ + NaCl) solutions. Corros. Sci. 38(4), 623-633.

Cheng, W., Marsac, R. and Hanna, K., 2018. Influence of magnetite stoichiometry on the binding of emerging organic contaminants. Environ. Sci. Technol. 52(2), 467-473.

Guilbaud, R., White, M.L. and Poulton, S.W., 2013. Surface charge and growth of sulphate and carbonate green rust in aqueous media. Geochim. Cosmochim. Acta. 108, 141-153.

Halevy, I., Alesker, M., Schuster, E.M., Popovitz-Biro, R. and Feldman, Y., 2017. A key role for green rust in the Precambrian oceans and the genesis of iron formations. Nature Geosci. 10(2), 135-139.

Hua, Y., Wang, W., Huang, X., Gu, T., Ding, D., Ling, L. and Zhang, W.X., 2018. Effect of bicarbonate on aging and reactivity of nanoscale zerovalent iron (NZVI) toward uranium removal. Chemosphere. 201, 603-611.

Jorge, J., Flahaut, E., Gonzalez-Jimenez, F., Gonzalez, G., Gonzalez, J., Belandria, E., Broto, J.M. and Raquet, B., 2008. Preparation and characterization of α-Fe nanowires located inside double wall carbon nanotubes. Chem. Phys. Lett. 457(4-6), 347-351.

Kanel, S.R., Nepal, D., Manning, B. and Choi, H., 2007. Transport of surface-modified iron nanoparticle in porous media and application to arsenic(III) remediation. J. Nanopart. Res. 9(5), 725-735.

Noubactep, C., 2013. An analysis of the evolution of reactive species in Fe^0/H_2O systems. J. Hazard. Mater. 168(2-3), 1626–1631.

Pedersen, O., Colmer, T. and Sand-Jensen, K., 2013. Underwater photosynthesis of submerged plants – recent advances and methods. Front. Plant. Sci. 4(140).

Schwertmann, U. and Fechter, H., 1994. The formation of green rust and its transformation to lepidocrocite. Clay Miner. 29(1), 87-92.

Shao, H., Qafoku, N.P., Lawter, A.R., Bowden, M.E. and Brown, C.F., 2015. Coupled geochemical impacts of leaking CO_2 and contaminants from subsurface storage reservoirs on groundwater quality. Environ. Sci. Technol. 49(13), 8202-8209.

Zhang, Y., Charlet, L. and Schindler, P.W., 1992. Adsorption of protons, Fe(II) and Al(III) on lepidocrocite (γ-FeOOH). Colloid Surf. 63(3), 259-268.